https://doi.org/10.5194/acp-2021-157
Preprint. Discussion started: 22 March 2021

Atmospheric Chemistry and Physics Discussions

Reproducing springtime Arctic tropospheric ozone depletion events in an outdoor mesocosm sea-ice facility

Zhiyuan Gao[1], Nicolas-Xavier Geilfus[1], Alfonso Saiz-Lopez[2], and Feiyue Wang[1]

[1]Centre for Earth Observation Science, and Department of Environment and Geography, University of Manitoba, Winnipeg, MB R3T 2N2, Canada
[2]Department of Atmospheric Chemistry and Climate, Institute of Physical Chemistry Rocasolano, CSIC, 28006 Madrid, Spain

Correspondence: Feiyue Wang (feiyue.wang@umanitoba.ca)

Abstract. The episodic build-up of gas-phase reactive bromine species over sea ice and snowpack in the springtime Arctic plays an important role in the boundary layer, causing annual concurrent depletion of ozone and gaseous elemental mercury during polar sunrise. Extensive studies have shown that these phenomena, known as bromine explosion events (BEEs), ozone depletion events (ODEs) and mercury depletion events (MDEs), respectively, are all triggered by gas-phase reactive bromine species that are photochemically activated from bromide via multi-phase reactions under freezing air temperatures. However, major knowledge gaps exist in both fundamental cryo-photochemical processes causing these events and meteorological conditions that may affect their timing and magnitude. Here, we report an outdoor mesocosm-scale study in which we successfully reproduced ODEs at the Sea-ice Environmental Research Facility (SERF) in Winnipeg, Canada. By monitoring ozone concentrations inside large, acrylic tubes over bromide-enriched artificial seawater during entire sea ice freeze-and-melt cycles, we observed mid-day photochemical ozone loss in winter in the boundary layer air immediately above the sea ice surface in a pattern that is characteristic of BEE-induced ODEs in the Arctic. The importance of UV radiation and the presence of a condensed phase (experimental sea ice or snow) in causing such surface ozone loss was demonstrated by comparing ozone concentrations between UV-transmitting and UV-blocking acrylic tubes under different air temperatures. The ability of reproducing BEE-induced ODEs at a mesocosm scale in a non-polar region provides a new approach to systematically studying the cryo-photochemical and meteorological processes leading to BEEs, ODEs, and MDEs in the Arctic, their role in biogeochemical cycles across the ocean-sea ice-atmosphere interfaces, and their sensitivities to climate change.

1 Introduction

Every year during springtime in the Arctic, a series of episodic photochemical events are observed concurrently in the boundary layer air, including bromine explosion events (BEEs), ozone depletion events (ODEs) and mercury depletion events (MDEs) (Barrie et al., 1988; Barrie and Platt, 1997; Bottenheim et al., 1986; Oltmans et al., 1989; Oltmans and Komhyr, 1986; Platt and Hausmann, 1994; Schroeder et al., 1998; Steffen et al., 2005). Subsequent studies have shown that these events are triggered by rapid cycling of photolytically activated halogen species (especially bromine species such as Br, BrO, HOBr, giving rise to BEEs) over sea ice or snowpack surface, which rapidly react with ozone and gaseous elemental mercury in the

https://doi.org/10.5194/acp-2021-157
Preprint. Discussion started: 22 March 2021

Atmospheric Chemistry and Physics Discussions

boundary layer air, resulting in ODEs and MDEs (Abbatt et al., 2012; Bognar et al., 2020; Pratt et al., 2013; Saiz-Lopez and von Glasow, 2012; Simpson et al., 2007; Wang et al., 2019). These annually recurring photochemical processes greatly change the oxidative conditions of the Arctic marine boundary layer during springtime, affecting biogeochemical cycles of many inorganic and organic chemicals across the ocean-sea ice-atmosphere interfaces in the Arctic (Wang et al., 2017).

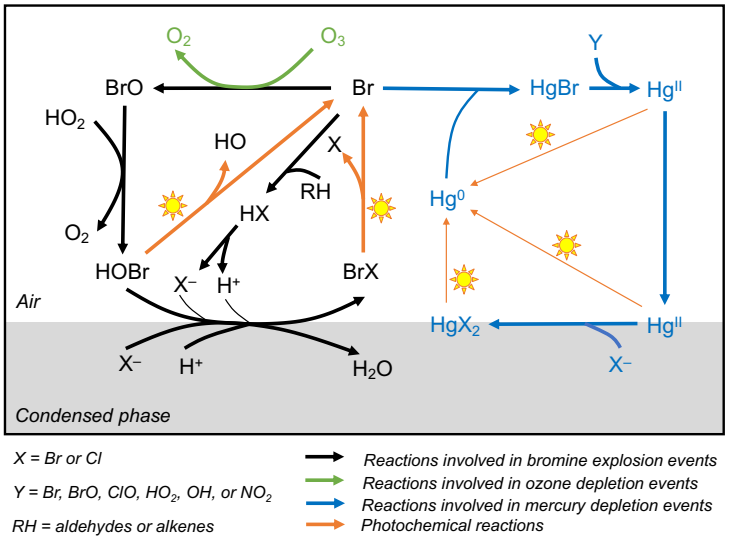

Figure 1. General reaction schemes involved in bromine explosion events, ozone depletion events and mercury depletion events in the Arctic during polar sunrise: gas-phase reactive bromine species (Br and BrO) produced from multi-phase reactions on the surface of the condensed phase will cause the depletion of ozone and gaseous elemental mercury in the boundary layer air (based on Abbatt et al., 2012; Saiz-Lopez and von Glasow, 2012; Simpson et al., 2007, 2015; Wang et al., 2017).

While there is a general consensus on the reaction schemes involved in BEEs, ODEs and MDEs (Fig. 1), major uncertainties exist with respect to the fundamental cryo-photochemical process causing these events and meteorological conditions that may affect their timing and magnitude. For instance, the initiation step is thought to be a multi-phase (mp) oxidation of halide by HOBr presumably on the surface of a saline condensed phase (Abbatt et al., 2012; Simpson et al., 2007, 2015):

$$X^- + HOBr + H^+ \xrightarrow{mp} H_2O + BrX \qquad (R1)$$

where X = Br or Cl. Yet the nature of the condensed phase remains not well characterized. Saline snowpack, first-year and multi-year sea ice, frost flowers and sea salt aerosols have all been proposed to provide such a condensed phase (Bognar et al., 2020; Pratt et al., 2013; Simpson et al., 2007, 2015; Wang et al., 2019). However, as Reaction (R1) is favoured under acidic conditions, the surfaces of sea ice and frost flowers, which are highly alkaline (Hare et al., 2013), are unlikely to be effective

https://doi.org/10.5194/acp-2021-157
Preprint. Discussion started: 22 March 2021


Atmospheric Chemistry and Physics Discussions

in initiating the reactions. Bromine activation also requires solar radiation, especially in the UV region, and is affected by air temperatures, as BEEs, ODEs and MDEs are only observed during polar sunrise and diminished when the air temperature rises to above 0 °C (Bognar et al., 2020; Steffen et al., 2005). Atmospheric and sea-state conditions, such as air mass origin, sea ice and boundary layer dynamics, and blowing snow events, may also affect the timing and magnitude of BEEs, ODEs and MDEs (Bognar et al., 2020; Moore et al., 2014; Thomas et al., 2011; Zhao et al., 2016).

So far most of the studies on BEEs, ODEs and MDEs are based on field observations, which reflect integrated complex processes occurring in nature, but the lack of controllability makes it difficult to address some of the aforementioned knowledge gaps on fundamental cryo-photochemical processes. The logistics of field campaigns also pose restrictions on the chemical species that can be measured and the nature and dynamics of the sea ice environment that can be studied. To help elucidate fundamental processes, laboratory studies have been conducted to study the halogen release mechanisms from frozen saline solutions (Abbatt et al., 2010; Huff and Abbatt, 2002; Sjostedt and Abbatt, 2008). Such frozen saline solutions may chemically resemble Arctic sea ice or snow substrates, but the laboratory-based studies cannot reproduce the natural growth of sea ice, nor the atmospheric and sea-state conditions. In this study, we present a mesocosm-scale experiment to investigate the occurrence and magnitude of BEE-induced ODEs. The experiment covered several freeze-and-melt cycles of experimental sea ice and open water periods. The temporal change in surface ozone concentrations was monitored in the boundary layer air mass inside acrylic tubes. Photochemical surface ozone loss under freezing air temperatures were observed in agreement with the characteristics of BEE-induced ODEs. We show that the experimental design provides a new platform to study mesocosm-scale BEEs, ODEs and MDEs, which will help elucidating fundamental processes behind their occurrence in the Arctic and their sensitivity to climate change.

2 Methods

2.1 Experimental set-up

The mesocosm experiment was carried out in winter (January–March) and fall (October) of 2020 at the Sea-ice Environmental Research Facility (SERF; 49.80 °N, 97.14 °W) located on the campus of the University of Manitoba, Winnipeg, Canada, more than 1,800 km south from the Arctic Circle. As the first experimental sea-ice facility in Canada, SERF has been supporting process-oriented, mesocosm-scale sea ice studies since 2012. It is equipped with an outdoor pool (18.3 m long, 9.1 m wide and 2.6 m deep) exposed to the ambient environment. The pool is filled with artificial seawater (~380 m^3) that resembles the salinity and major ionic composition of Arctic seawater. As the air temperature drops well below 0 °C (down to –30 °C) in winter, the experimental sea ice exhibits similar physical and chemical properties to natural first-year sea ice in the Arctic Ocean (Geilfus et al., 2016; Hare et al., 2013; Xu et al., 2016).

The artificial seawater was prepared in November 2019 and formulated by mixing groundwater with concentrated NaCl brine and secondary salts ($MgCl_2$•$6H_2O$, $MgSO_4$•$7H_2O$, $CaCl_2$ and NaBr) to achieve a major-ion composition resembling that of the standard seawater (Millero, 2013) at a salinity of 32.8, including chloride (532 mmol kg^{-1}), sulphate (28.4 mmol kg^{-1}),

https://doi.org/10.5194/acp-2021-157
Preprint. Discussion started: 22 March 2021

Atmospheric Chemistry and Physics Discussions

sodium (495 mmol kg^{-1}), calcium (10.3 mmol kg^{-1}) and magnesium (33.2 mmol kg^{-1}). To create an amplified signal of bromine activation, excess bromide was added to reach a final concentration of 6.52 mmol kg^{-1}, which is ~ 8.2 times that (0.79 mmol kg^{-1}) of a S=32.8 seawater. The artificial seawater was left to equilibrate with the atmosphere for more than one month. To prevent it from freezing, seawater was heated from the bottom of the pool and continuously mixed using circulation pumps until the start of the experiments. At the end of the equilibration (21 January 2020), the artificial seawater had a pH of 7.75, a dissolved inorganic carbon (DIC) concentration of 2500 µmol kg^{-1} and total alkalinity (TA) of 2544 µmol kg^{-1}.

In total, three experiments focusing on different ice or open water stages were carried out. Two of them (Experiments #1 and #2) followed successive freeze-and-melt cycles of experimental sea ice during the winter, and the third one (Experiment #3) was carried out in the fall with open water. Experiment #1 started on 21 January when the heater and circulation pump were turned off. The ice grew naturally until 22 February when the heating on the bottom of the pool was turned on to melt the ice. Open water first appeared on 24 February at which time the circulation pump was turned on to speed up the melting process. The pool became completely ice free on 2 March. After the heating and circulation pump were turned off, Experiment #2 started on the same day and continued until 17 March. It followed a natural melting process as the weather warmed up near the end of the experiment. Experiment #3 was carried out in October 2020 for two weeks and the pool remained ice free throughout the duration.

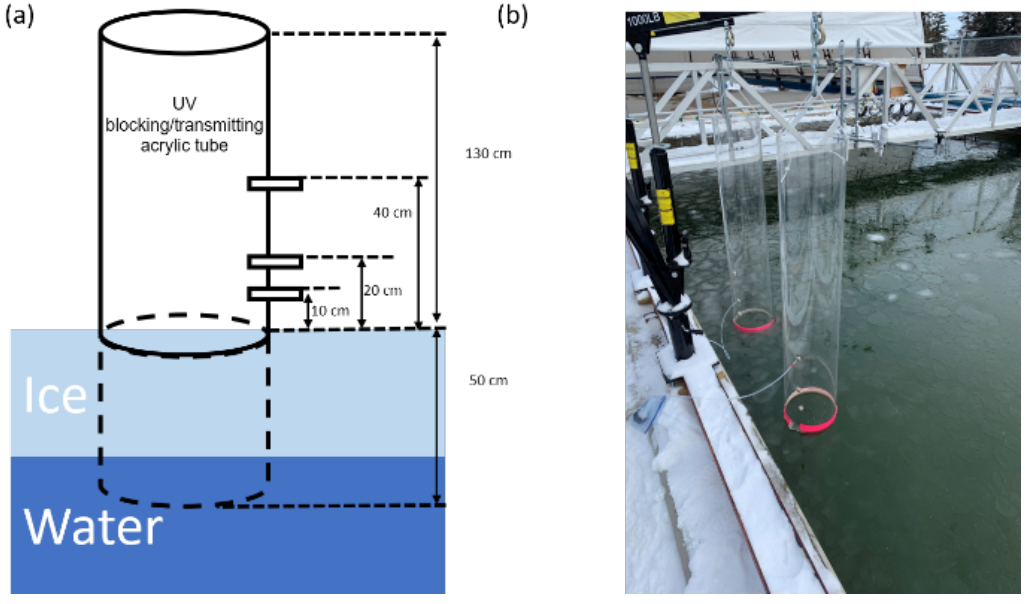

Figure 2. (a) An illustration and (b) a photo showing the experimental set-up at the Sea-ice Environmental Research Facility, Winnipeg, Canada. Two acrylic tubes (one UV-blocking and the other UV-transmitting) were fixed vertically in the sea ice pool, with ozone measurement ports drilled at various heights through the tube wall.

https://doi.org/10.5194/acp-2021-157
Preprint. Discussion started: 22 March 2021


Atmospheric Chemistry and Physics Discussions

Due to the small surface area of the SERF pool (167 m^2) in the otherwise urban environment far away from the Arctic, chemical change in the boundary layer air over the pool can be greatly interfered by the mixing with the ambient air. To limit such air mixing and be able to monitor the change in the ozone concentration immediately above the seawater or sea ice surface, two large acrylic tubes (inner diameter: 30 cm, height: 183 cm; Emco Industrial Plastics, Cedar Grove, NJ) were fixed into the seawater before it was frozen, with the bottom 50 cm being submerged in the water. They were placed about 30 cm away from the edge of the pool and were kept vertical by mechanical arms fixed on the edge of the pool (Fig. 2). One of the tubes was made of UV-blocking acrylic material (cut-off wavelength: 370 nm), and the other of UV-transmitting acrylic material (cut-off wavelength: 270 nm) (see Fig. S1). On each tube, three brass adaptors were drilled through the acrylic wall as sampling ports on the same side located at 10 cm, 20 cm and 40 cm above the water surface, permitting real-time ozone measurements in the boundary layer air at different heights (Fig. 2). For the rest of this paper, the "boundary layer air" is referred to the air mass above the sea ice surface inside the tubes, whereas the air outside of the tubes is considered the "ambient air".

2.2 Ozone measurements

Real-time ozone concentrations in the boundary layer air and ambient air were measured using a Teledyne T400 ozone analyzer at every minute. The flow rate was 0.8 L min^{-1} through a 4-m sample line (inner diameter: 4.8 mm). The ozone analyzer was calibrated at the beginning of the experiment, and frequently checked at a span range of 450 ppb. The relative standard deviation for the span check during the experiments was 2.1 % (n = 11). To allow ozone measurement of the boundary layer air in different tubes or at different heights above the surface, a Tekran 1100 dual port module was used to automatically switch between the sampling ports on the two tubes at an interval of 5 minutes. Thus, the ozone data reported herein are averaged over a 5-min integration time. The ozone concentrations in the ambient air near the pool were also measured during the experiments.

The quantify and normalize the ozone difference inside UV-transmitting tube relative to other locations, the ozone loss (%) is reported and calculated by Eq (1):

$$\Delta O_3(\%) = \frac{[O_3]_i - [O_3]_{UVT}}{[O_3]_i} \times 100\% \quad (1)$$

where $[O_3]_i$ is the ozone concentration in the ambient air or inside the UV-blocking tube, and $[O_3]_{UVT}$ is the ozone concentration inside the UV-transmitting tube.

2.3 Other measurements

Meteorological conditions were measured at a station located at 1.5 m above the ice surface, including air temperature by a Vaisala HMP45C probe, solar irradiance by a CNR4 net radiometer (Kipp & Zonen, spectral range of 0.3–2.8μm), and wind by an UltraSonic anemometer (WindSonic). In situ sea ice and seawater temperatures were measured by an automated type-T thermocouple array installed vertically throughout the depth of the pool at a resolution of 2 cm for the top 50 cm.

https://doi.org/10.5194/acp-2021-157
Preprint. Discussion started: 22 March 2021


Atmospheric Chemistry and Physics Discussions

Seawater, sea ice and snow samples were collected discretely for major ion, DIC and TA analysis. Two ice cores were collected for major ion analysis using a Mark II coring system (diameter: 9 cm; KOVACS Enterprise, Roseburg, OR) at the middle and end of Experiment #1 on 10 February and 21 February, respectively. More frequent ice core collection was conducted for DIC and TA measurement. Ice cores were taken from outside of the acrylic tubes within a few meters from where the tubes were located and cut into 3-cm sections immediately after the retrieval. Ice sections were stored in gas-tight plastic bags (Nylon/poly, Cabela's) and vacuum-sealed (Hu et al., 2018), followed by melting at 4 °C in the dark until further analysis. Under-ice water was sampled for major ion analysis by submerging 50-mL polypropylene tubes (Falcon) completely underwater from the hole where the ice core was taken, after manually clearing off floating ice. For DIC and TA measurement, the water samples were collected in 100-mL incubation bottles. Multiple snow samples were taken within 48 hours after the snow deposition by scooping untouched surface snow on sea ice within the pool area and on the nearby land into 50-mL Falcon tubes.

Seawater, melted sea ice and snow samples were analyzed for major ions including bromide by ion chromatography (IC) on a DIONEX 5000+ IC system. The recovery and method of detection limit (MDL) were determined from repetitive measurements on a Dionex seven anion standard and a Dionex six cation-II standard, and were 98 % and 1.46 μmol kg^{-1} for bromide, 96 % and 1.96 μmol kg^{-1} for chloride, 99 % and 3.05 μmol kg^{-1} for sulphate, 107 % and 0.20 μmol kg^{-1} for sodium, 119 % and 0.79 μmol kg^{-1} for magnesium, and 93 % and 0.95 μmol kg^{-1} for calcium. Water aliquots were also collected to measure salinity. Salinity was calculated from conductivity (Grasshoff et al., 2007), which was measured by a conductivity cell probe (Orion 013610MD, Thermo Scientific).

The analysis of DIC and TA followed the process as described in Geilfus et al. (2016). Briefly, ice samples were melted at 4 °C in the dark to minimize the possible dissolution of ikaite crystals. Once sea ice melted, meltwater and seawater were processed similarly by transferring to gas-tight vials (12-mL Exetainers, Labco High Wycombe, UK), preserved with 12 μL solution of saturated $HgCl_2$, and stored at room temperature in the dark until analysis. Total alkalinity was determined by Gran titration (Gran, 1952) on a TIM 840 titration system (Radiometer Analytical, ATS Scientific) (Hu et al., 2018). A 12-mL sample was titrated with a standard 0.05 M HCl solution (Alfa Aesar). Dissolved inorganic carbon was measured on a DIC analyzer (Apollo SciTech) by acidifying a 0.75 mL subsample with 1 mL 10 % H_3PO_4 (Sigma-Aldrich), followed by quantifying the released CO_2 with a CO_2 analyzer (LI-COR, LI-7000). Results were then converted from μmol L^{-1} to μmol kg^{-1} based on sample density, which was estimated from salinity and temperature at the time of the analysis. Accuracies of ± 3 and ± 2 μmol kg^{-1} were determined for TA and DIC, respectively, from analysis of certified reference materials (A.G. Dickson, Scripps Institution of Oceanography, USA).

2.4 Statistical analysis

Statistical analysis was carried out using Microsoft Office Excel. One-way ANOVA was used to examine the statistical difference under different occasions and the significant level was set at 0.05 for each test.

https://doi.org/10.5194/acp-2021-157
Preprint. Discussion started: 22 March 2021


Atmospheric Chemistry and Physics Discussions

3. Results

3.1 Meteorological, sea ice and snow properties

Solar radiation, wind speed and the temperatures of the ambient air, sea ice (when present) and seawater are shown in Fig. 3 and Fig. S2. Throughout Experiments #1 and #2, the presence and vertical extent of sea ice is approximated by the – 2 °C isothermal (Fig. 3c) in the pool.

During Experiment #1 (24 January to 22 February), the ambient air temperature dropped below – 30 °C and the pool surface was completely ice-covered for the entire experiment. The temperature of surface sea ice reached as low as – 16 °C on 19 February. Maximal ice thickness (~ 27 cm) was reached on 21 February near the end of Experiment #1. The daytime that is characterized by a positive downward shortwave radiation was ~10 hours (from ~8:00 to ~18:00; all time local = UTC – 6 hr). During Experiment #2 (3 to 17 March), the ambient air temperature increased gradually from – 20 °C to – 10 °C (Fig. 3). The pool surface was only partially sea ice covered as a result of warming weather that caused interrupted freezing period. The sea ice (when present) thickness was typically less than 10 cm. A longer daytime was observed (~11 hours), from ~7:00 to ~18:00. During Experiment #3 (19 to 30 October), no sea ice was observed within the pool. The ambient air temperature ranged from – 8 °C to 4 °C, and the daytime lasted ~9.5 hours (from ~7:30 to ~17:00).

During Experiments #1 and #2, flurries of snow occurred episodically with less than 1 cm of snow accumulation within the pool area, except on 15 February when up to 5 cm of snow was accumulated on the ice cover during a snowfall event. The deposited snow went through diel cycle of melting and re-freezing to eventually form a crust layer on the sea ice surface or was blown away from the SERF pool by wind turbulence within 24 hours after deposition. Yet, the accumulated snow layer (< 2 cm) inside the tubes remained visible for several days on the ice surface and inner tube walls as it was sheltered from the ambient wind.

3.2 Ozone in the boundary layer air and ambient air

Ozone concentrations in the ambient air and in the boundary layer air inside UV-transmitting and UV-blocking tubes (at 10 cm above the ice surface) are shown in Fig. 3. Large temporal variations in ozone concentrations were found in both the boundary layer air inside the UV-transmitting tube and ambient air, ranging from 0 to 50 ppb, yet they showed similar temporal patterns. During the overlapped data collection period (17 to 20 February and 3 to 17 March), ozone in the ambient air (32.9 ± 8.5 ppb; mean ± standard deviation) was slightly but significantly higher than that in the boundary layer air measured at 10 cm above the ice surface (30.8 ± 8.2 ppb) ($p = 0.00$).

Comparisons of ozone concentrations in the boundary layer air inside UV-transmitting and UV-blocking tubes are shown in Fig. 4. Ozone was measured at different heights (10, 20, 40 cm) above the sea ice surface during Experiment #1, whereas during Experiment #3 all the measurements were done at 10 cm above the water surface. The boundary layer ozone concentrations between the two tubes were not significantly different when measured at 40 cm ($p = 0.33$) and 20 cm ($p = 0.83$) above the sea ice surface during Experiment #1 (Fig. 4a, b), or at 10 cm above the water surface during Experiment #3 ($p =$

https://doi.org/10.5194/acp-2021-157
Preprint. Discussion started: 22 March 2021

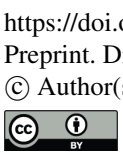

Atmospheric Chemistry and Physics Discussions

0.11) (Fig. 4c). The only exception is the measurement conducted closest to the sea ice surface (10 cm) during the ice-covered
200 period in Experiment #1, when the ozone concentration in the UV-transmitting tube was consistently and considerably lower than that in the UV-blocking tube ($p = 0.00$) (Fig. 4c).

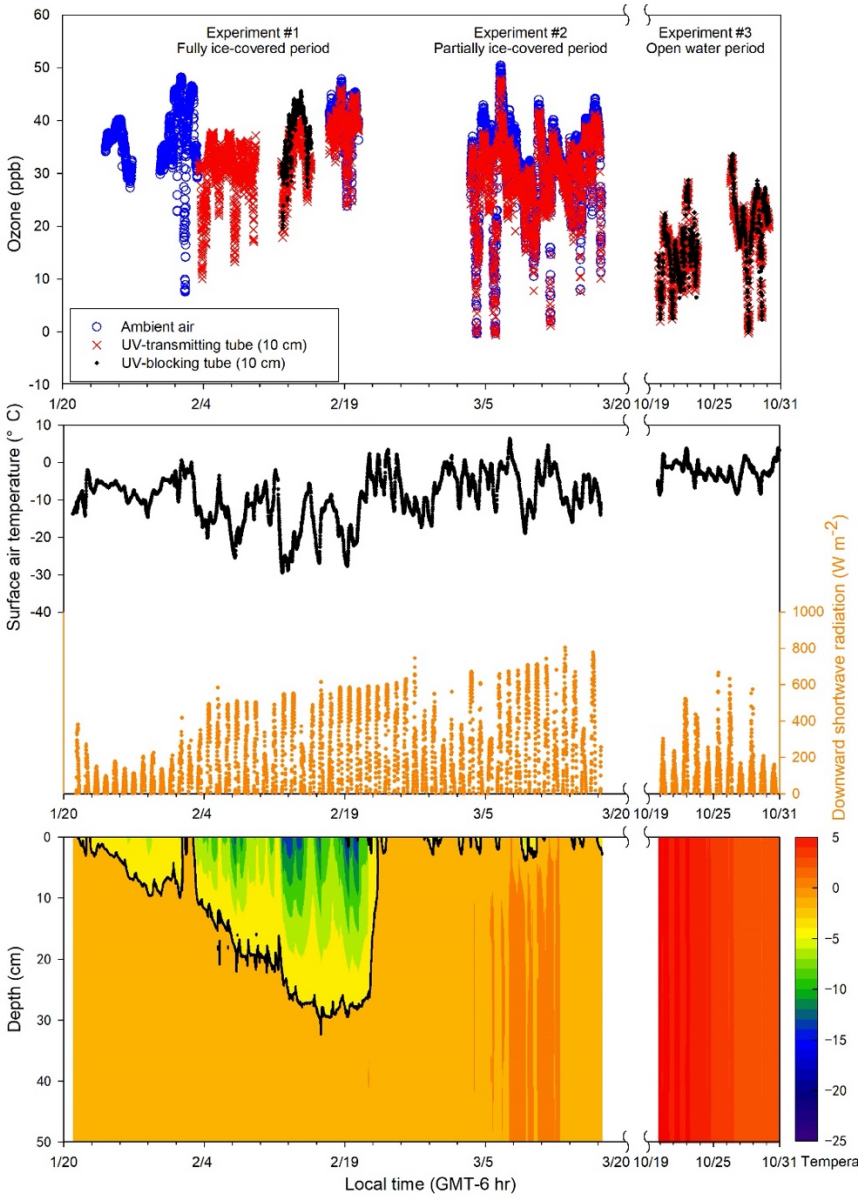

Figure 3. Temporal changes of (a) ozone in ambient air, UV-transmitting and UV-blocking tube (10 cm above the ice or water
205 surface); (b) surface air temperature, solar radiation (1.5 m above the ice or water surface), and (c) ice and water temperatures in the top 50 cm of the pool.

https://doi.org/10.5194/acp-2021-157
Preprint. Discussion started: 22 March 2021

Atmospheric Chemistry and Physics Discussions

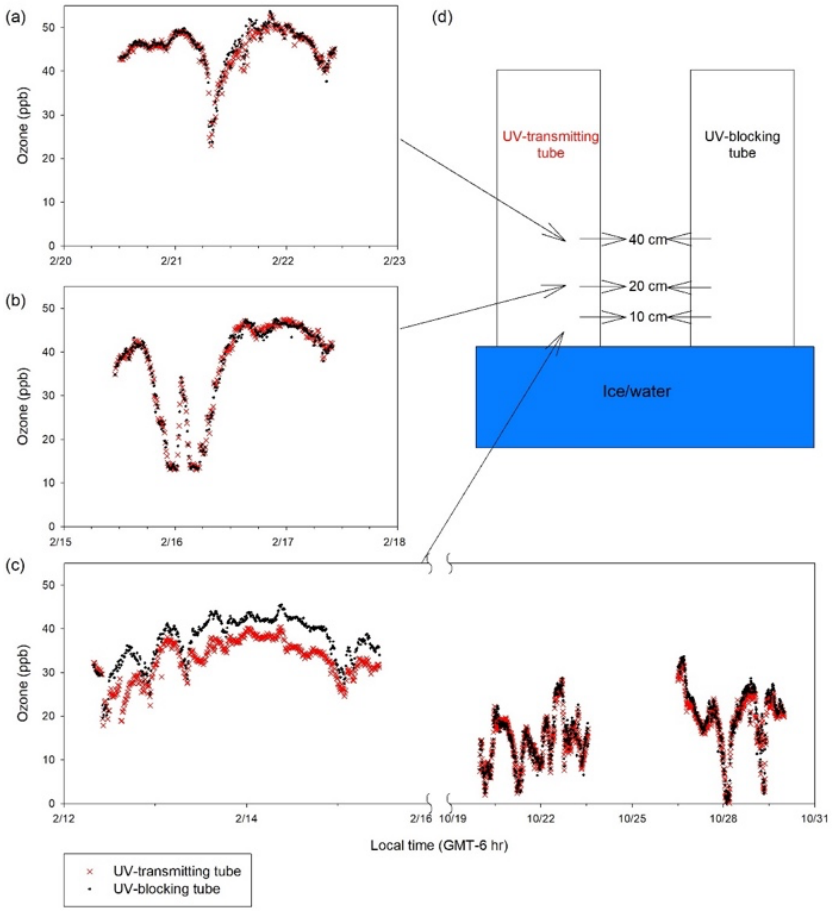

Figure 4. Ozone concentrations in the boundary layer air inside the UV-transmitting and UV-blocking tubes as measured at (a) 40 cm, (b) 20 cm, and (c) 10 cm above the ice (or water) surface. The measurement schemes are illustrated in (d).

3.2 Chemical composition of sea ice and snow

As expected, considerable amounts of major ions from seawater are retained in sea ice (Table 1). Major ion concentrations are very low in snow collected from nearby land surfaces, whereas considerably (~ 100 times) higher concentrations are found for the thin layer of snow above sea ice, which is consistent with the brine-wetting process in snow overlying sea ice (Barber and Nghiem, 1999). Bromide is of particular interest, which was found to be preferentially enriched in sea ice and in the overlying snow, as demonstrated by elevated Br^-/Na^+ molar ratio (0.020 and 0.017, respectively) when compared with that in the underlying seawater (0.013). Similar preferential enrichment was not observed for other major ions.

https://doi.org/10.5194/acp-2021-157
Preprint. Discussion started: 22 March 2021

Atmospheric Chemistry and Physics Discussions

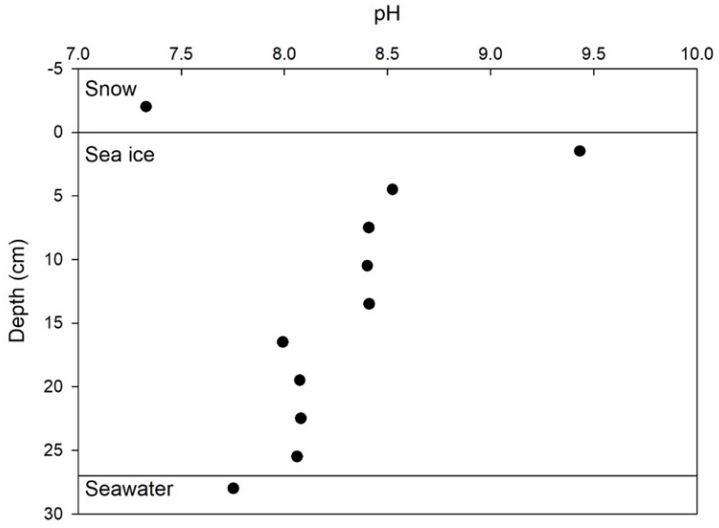

220 **Figure 5.** Vertical profile of pH across the snow-sea ice-seawater interface, as measured on 21 February 2020.

The vertical profile of pH across the snow-sea ice-seawater interface was measured only once on 21 February (Fig. 5). The pH of the sea ice changed from 8.06 at the bottom, to 7.99 in the mid-section, and as high as 9.43 near the surface. Estimate based on the measurements of salinity, DIC and TA (Table 2) suggests that the thin ice and the surface layer of the growing
225 ice consistently had a pH > 8.5 during Experiment #1. Both the high pH values at the surface and the C-shaped vertical distribution pattern are in good agreement with those reported in a previous mesocosm study at SERF (Hare et al., 2013). The snow overlying sea ice had a pH of 7.2. It is not as acidic as expected from that of fresh snow (6.74) due to the influence of sea ice brine, but still more than 1-2 orders of magnitude more acidic than the surface sea ice.

230 **Table 1.** Major-ion composition of snow, surface ice and surface seawater during Experiment #1

	Concentration (mmol kg^{-1})						Molar ratio				
	Cl^-	Br^-	SO_4^{2-}	Na^+	Mg^{2+}	Ca^{2+}	Br^-/Na^+	Cl^-/Na^+	SO_4^{2-}/Na^+	Mg^{2+}/Na^+	Ca^{2+}/Na^+
Snow over land (n=8)	1.48 ± 0.80	0.002 ± 0.001	0.014 ± 0.003	0.38 ± 0.20	0.03 ± 0.02	0.07 ± 0.02	4.36 ± 2.16	0.003 ± 0.000	0.11 ± 0.11	0.06 ± 0.03	0.19 ± 0.09
Snow over sea ice (n=11)	290 ± 105	4.32 ± 2.11	16.5 ± 5.6	261 ± 96	19.8 ± 9.8	5.8 ± 2.2	1.12 ± 0.04	0.017 ± 0.007	0.07 ± 0.02	0.04 ± 0.03	0.02 ± 0.00
Sea ice (top 3 cm) (n=4)	269 ± 23	4.88 ± 1.72	17.9 ± 0.8	251 ± 20	18.1 ± 3.0	5.0 ± 0.6	1.07 ± 0.01	0.020 ± 0.008	0.07 ± 0.00	0.07 ± 0.01	0.02 ± 0.00
Surface seawater (n=3)	532 ± 8	6.52 ± 1.06	28.4 ± 1.1	495 ± 2	33.2 ± 16.6	10.3 ± 0.21	1.07 ± 0.01	0.013 ± 0.002	0.06 ± 0.00	0.07 ± 0.03	0.02 ± 0.00

https://doi.org/10.5194/acp-2021-157
Preprint. Discussion started: 22 March 2021

Atmospheric Chemistry and Physics Discussions

Table 2. Dissolved inorganic carbon (DIC) and total alkalinity (TA) of the seawater and sea ice during Experiment #1

Date	Depth (cm)	Salinity	TA (μmol kg^{-1})	DIC (μmol kg^{-1})
Seawater:				
21 January		32.8	2544	2500
Sea ice:				
22 January	bulk	15.6	1256	1267
24 January	bulk	13.4	1053	877
27 January	bulk	12.3	994	438
30 January	0–4	5.6	484	824
5 February	0–5	7.3	609	518
7 February	0–5	8.0	692	623
10 February	0–5	7.4	670	532
14 February	0–5	9.2	759	604
20 February	0–5	6.3	519	491
24 February	0–5	10.3	844	790

4. Discussion

4.1 Cryo-photochemically driven ozone loss in the boundary layer air

The temporal variations of ozone concentrations in the ambient air at SERF (Figs. 3a and 6a) agree well with those reported for Canadian cities (Angle and Sandhu, 1989; Raddatz and Cummine, 2001). On a diurnal basis (Fig. 6a), the ambient ozone concentration increases gradually after sunrise (~7:30), and peaked around 15:00–17:00, corresponding to the production of ozone during photochemical oxidation of hydrocarbons from automobile exhaust, which is also supported by the variation in downward shortwave radiation (Fig. 6c). After sunset, the ambient ozone concentrations increase slightly due to the inflow of ozone from surrounding rural areas as a result of nocturnal urban heat island effect (Raddatz and Cummine, 2001). Similar diurnal patterns of the ozone concentrations are evident in the boundary layer air inside the UV-transmitting tube even at 10 cm above the sea ice surface (Fig. 6a), suggesting that the ozone concentration is largely controlled by the urban signal. However, ozone concentrations in the ambient air are consistently higher than that inside the UV-transmitting

https://doi.org/10.5194/acp-2021-157
Preprint. Discussion started: 22 March 2021


Atmospheric Chemistry and Physics Discussions

tube during sun-lit, daytime (Fig. 6a). This could be indicative of limited mixing of the ambient air inside the tube due to the wall effect, and/or loss of ozone inside the tube due to the presence of the experimental sea ice.

To address which of these processes is primarily responsible for the observed ozone difference, we further compare the ozone concentrations measured inside the UV-blocking and UV-transmitting tubes. Although the overall temporal patterns between the two tubes are similar during Experiment #1 (Fig. 4), the ozone concentration in the boundary layer air immediately (10 cm) above the sea ice in the UV-transmitting tube are consistently and considerably lower than those in the UV-blocking tube (Fig. 4c). The associated ozone loss (ΔO_3) shows a clear diurnal pattern with the largest difference (> 25%) appearing in the early afternoon (12:00–15:00) that corresponds to the peak time of the downward shortwave radiation (Fig. 7). Since the major difference between the two tubes is their UV-transmitting ability in the range of 270 to 370 nm (Fig. S1), the considerable mid-day ozone loss inside the UV-transmitting tube can only be attributed to photochemical processes that are prohibited inside the UV-blocking tube.

The observation that no such ozone loss occurred in the boundary-layer air when measured farther away (20 cm and 40 cm) from the sea ice surface (Fig. 4a, b) suggests that the ozone loss is triggered by cryo-photochemical processes that involve the sea ice environment. At 20 cm or 40 cm above the sea ice surface, the ozone difference between the two tubes becomes indiscernible due to the faster mixing of the ozone-rich ambient air or lack of ozone-depleting processes away from the sea ice surface. The importance of cryo-photochemical processes in the ozone loss is further supported by Experiment #3 when the measurement was conducted in the absence of sea ice, as no ozone loss was observed even immediately (10 cm) above the water surface (Fig. 6c).

Since the UV-transmitting tube only has a UV transmittance of ~60% (Fig. S1), even higher magnitude of ozone loss is expected to occur outside the acrylic tubes over the entire SERF sea ice surface. However, the rapid mixing of the boundary layer air and ambient would readily bury the ozone-depleting signal under the much larger background of ambient urban air, making it difficult to directly observe such cryo-photochemical ozone loss. The use of the acrylic tubes is thus critical for the observation, as they limited the air mixing and permitted gas sampling from the boundary layer air mass that was directly affected by the sea ice surface.

4.2 Mesocosm reproduction of polar springtime photochemical phenomena

Although no direct measurements were made in this study on gas-phase bromine species in the air above sea ice or snow, we believe the cryo-photochemical ozone loss observed over the SERF pool is caused by the same mechanism involving bromine activation that is responsible for the Arctic springtime ODEs. The other known tropospheric ozone depletion mechanisms include direct photolysis (Schmidt et al., 2016; Wu et al., 2007) and ozone deposition on the tube walls, which are negligible at the study site (see Fig. 7c).

https://doi.org/10.5194/acp-2021-157
Preprint. Discussion started: 22 March 2021

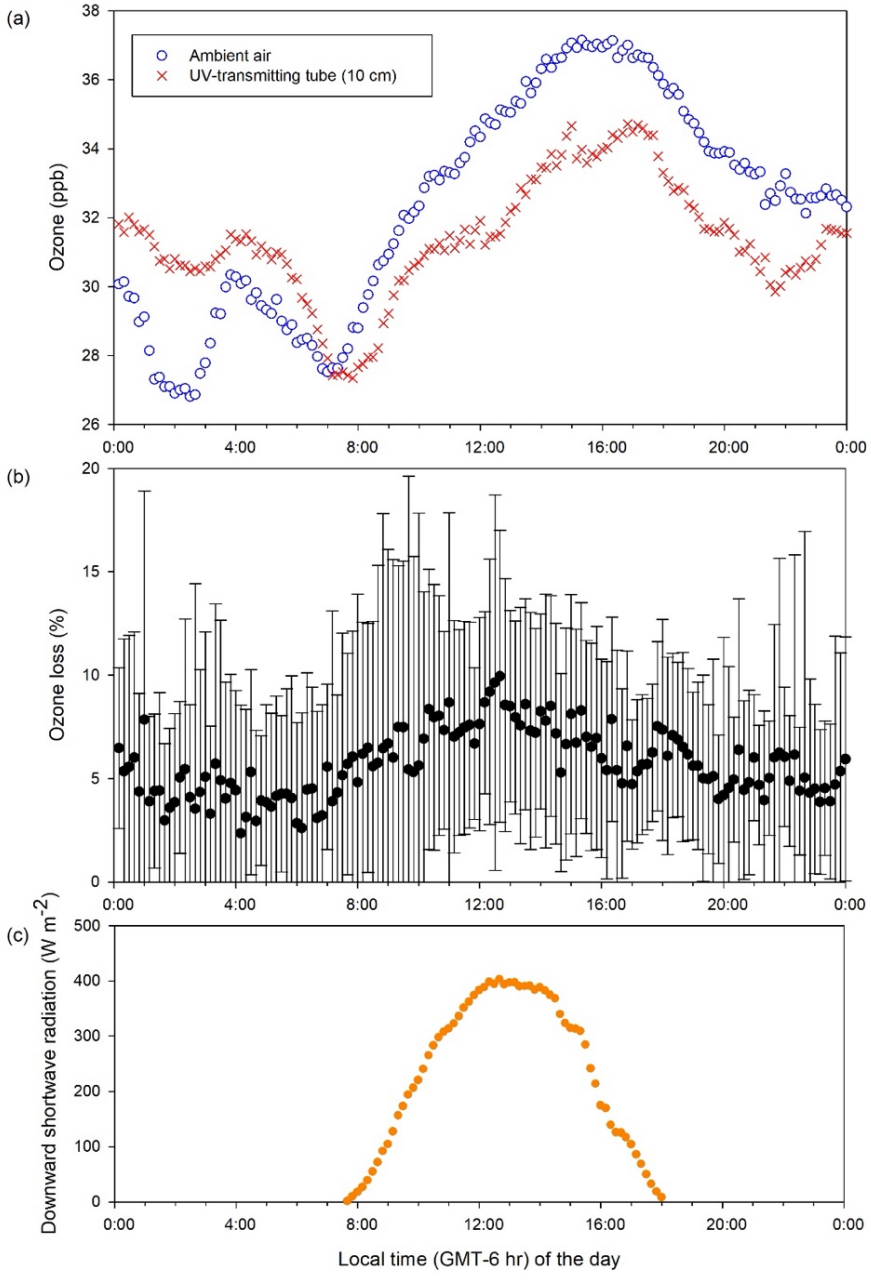

Figure 6. Diurnal patterns (averaged over 24 January to 17 March whenever the measurement was available) of (a) ozone concentrations in the ambient air and boundary layer air inside the UV-transmitting tube (10 cm above the sea ice), (b) ozone loss (measured as the ozone concentration difference between the ambient and boundary layer air inside UV-transmitting tube), and (c) downward shortwave radiation.

https://doi.org/10.5194/acp-2021-157
Preprint. Discussion started: 22 March 2021

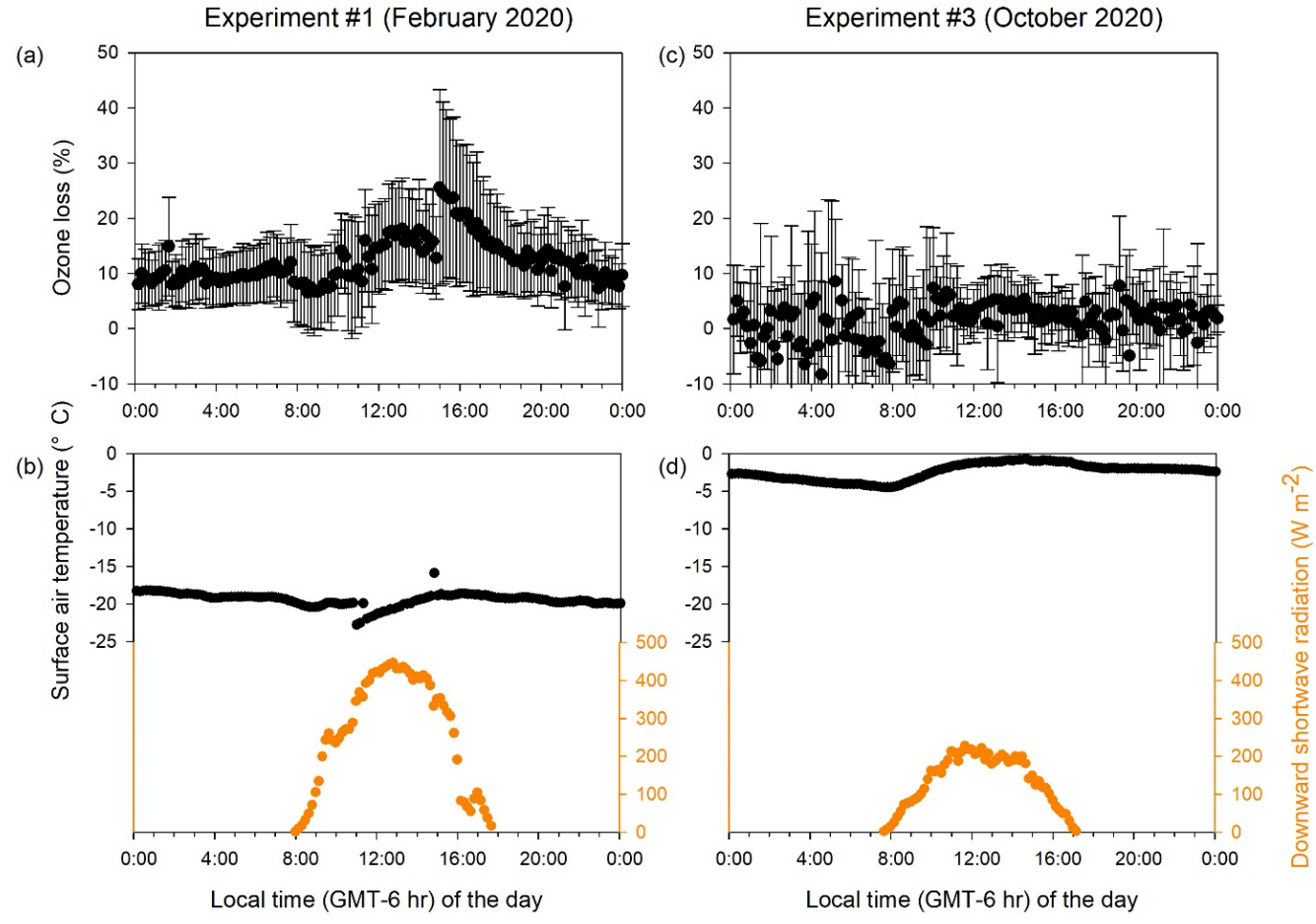

Figure 7. Diurnal patterns of (a, c) ozone loss (measured as the ozone concentration difference in the boundary layer air between UV-transmitting and UV-blocking tubes at 10 cm above the sea ice or water surface), and (b, d) meteorological conditions during the ice-covered (a, b) and open water (b, d) experiments.

As shown in Fig. 1, Br radicals-induced cryo-photochemical ozone loss involves multi-phase reactions on the surface of a condensed phase under acidic conditions (Abbatt et al., 2012; Pratt et al., 2013; Simpson et al., 2007). The condensed phase can be either the bare sea ice or the thin layer of snow accumulated on the sea ice surface at the second half of Experiment #1. However, the highly alkaline nature of the sea ice surface (Fig. 5; see also Hare et al., 2013) suggests it is not the most efficient surface where bromide activation takes place. Instead, the overlying snow is more likely acting as the condensed phase for the reactions to take place, as it is more acidic (Fig. 5) yet enriched in bromide (Table 1) due to upward migration of sea ice brine. As shown in Table 1, the bromide added in the artificial seawater eventually contributed to enriched bromide concentrations found in sea ice surface and the overlying snowpack, providing abundant substrates for bromine activation.

https://doi.org/10.5194/acp-2021-157
Preprint. Discussion started: 22 March 2021


Atmospheric Chemistry and Physics Discussions

5. Conclusion

In this paper, we show that the Arctic springtime ODEs can be reproduced in a mesocosm-scale experiment in an outdoor sea ice facility located in an urban area far away from the Arctic. By constraining the boundary layer air mass within a UV-transmitting tube, cryo-photochemical ozone loss above experimental sea ice is observed with a diurnal pattern that is characteristic of BEE-induced ODEs. The comparison between UV-blocking and UV-transmitting acrylic tubes further emphasizes the role of UV radiation (270 to 370 nm) in causing such ozone destruction.

The success in reproducing BEE-induced ODEs at the mesocosm scale provides a new approach that can supplement, bridge and integrate the laboratory and field-scale studies to advance our understanding of the cryo-photochemical and meteorological processes leading to BEEs, ODEs, and MDEs in the Arctic. In addition to much simpler logistical preparations, major advantages of the mesocosm-scale approach are the ability to control and modify the nature and dynamics of various condensed phases (e.g., sea ice, frost flowers, leads, overlying snow and blowing snow under various growth and melting conditions), the ability to dope or alter chemical composition of seawater and condensed phases (e.g., addition of bromide and mercury stable isotopes, acidity), the ability to control the light environment, and the accessibility to various monitoring and analytical capacities that are difficult to access in the remote Arctic. The results will not only help fill up critical knowledge gaps related to BEEs, ODEs and MDEs, but also aid the development and parameterization of mechanistic models to allow better projection of their sensitivities to climate change in the Arctic and implications for biogeochemical cycles across the ocean-sea ice-atmosphere interfaces.

Data availability

The datasets generated in this study are available on request from the corresponding author.

Author contribution

ZG and FW designed the experiments and led the data interpretation. ZG and NXG carried out the experiments. ASL assisted in data interpretation. ZG and FW prepared the manuscript with contributions from all co-authors.

Competing interests

The authors declare that they have no conflict of interest.

https://doi.org/10.5194/acp-2021-157
Preprint. Discussion started: 22 March 2021

Atmospheric Chemistry and Physics Discussions

Acknowledgements

This work was funded by the Natural Science and Engineering Council of Canada (NSERC), the Canada Research Chairs program, the Canada Excellence Research Chairs (CERC) program, and the University of Manitoba Graduate Fellowship. We thank D. Armstrong for assistance in the major ion analysis, and D. Binne for assistance in the experimentation at the Sea-ice Environmental Research Facility (SERF).

References

Abbatt, J., Oldridge, N., Symington, A., Chukalovskiy, V., McWhinney, R. D., Sjostedt, S. and Cox, R. A.: Release of gas-phase halogens by photolytic generation of OH in frozen halide-nitrate solutions: An active halogen formation mechanism? J. Phys. Chem. A, 114, 6527–6533, https://doi.org/10.1021/jp102072t, 2010.

Abbatt, J. P. D., Thomas, J. L., Abrahamsson, K., Boxe, C., Granfors, A., Jones, A. E., King, M. D., Saiz-Lopez, A., Shepson, P. B., Sodeau, J., Toohey, D. W., Toubin, C., von Glasow, R., Wren, S. N. and Yang, X.: Halogen activation via interactions with environmental ice and snow in the polar lower troposphere and other regions, Atmos. Chem. Phys., 12, 6237–6271, https://doi.org/10.5194/acp-12-6237-2012, 2012.

Angle, R. P. and Sandhu, H. S.: Urban and rural ozone concentrations in Alberta, Canada, Atmos. Environ., 23, 215–221, https://doi.org/10.1016/0004-6981(89)90113-3, 1989.

Barber, D. G. and Nghiem, S. V.: The role of snow on the thermal dependence of microwave backscatter over sea ice, J. Geophys. Res. Ocean., 104, 25789–25803, https://doi.org/10.1029/1999jc900181, 1999.

Barrie, L. and Platt, U.: Arctic tropospheric chemistry: An overview, Tellus, Ser. B Chem. Phys. Meteorol., 49, https://doi.org/10.3402/tellusb.v49i5.15984, 1997.

Barrie, L. A., Bottenheim, J. W., Schnell, R. C., Crutzen, P. J. and Rasmussen, R. A.: Ozone destruction and photochemical reactions at polar sunrise in the lower Arctic atmosphere, Nature, 334, 138–141, https://doi.org/10.1038/334138a0, 1988.

Bognar, K., Zhao, X., Strong, K., Chang, R. Y. W., Frieß, U., Hayes, P. L., McClure-Begley, A., Morris, S., Tremblay, S. and Vicente-Luis, A.: Measurements of tropospheric bromine monoxide over four halogen activation seasons in the Canadian High Arctic, J. Geophys. Res. Atmos., 125, 1–23, https://doi.org/10.1029/2020JD033015, 2020.

Bottenheim, J. W., Gallant, A. G. and Brice, K. A.: Measurements of NO_Y species and O_3 at 82° N latitude, Geophys. Res. Lett., 13, 113–116, https://doi.org/10.1029/GL013i002p00113, 1986.

Geilfus, N. X., Galley, R. J., Else, B. G. T., Campbell, K., Papakyriakou, T., Crabeck, O., Lemes, M., Delille, B. and Rysgaard, S.: Estimates of ikaite export from sea ice to the underlying seawater in a sea ice-seawater mesocosm, Cryosphere, 10, 2173–2189, https://doi.org/10.5194/tc-10-2173-2016, 2016.

Gran, G.: Determination of the equivalence point in potentiometric titrations. Part II, Analyst, 77, 661–670, https://doi.org/10.1039/AN9527700661, 1952.

Grasshoff, K., Kremling, K. and Ehrhardt, M.: Methods of Seawater Analysis, Third Edition, Wiley-VCH, Weinheim, 2007.

https://doi.org/10.5194/acp-2021-157
Preprint. Discussion started: 22 March 2021


Atmospheric Chemistry and Physics Discussions

Hare, A. A., Wang, F., Barber, D., Geilfus, N. X., Galley, R. J. and Rysgaard, S.: pH evolution in sea ice grown at an outdoor experimental facility, Mar. Chem., 154, 46–54, https://doi.org/10.1016/j.marchem.2013.04.007, 2013.

Hu, Y. Bin, Wang, F., Boone, W., Barber, D. and Rysgaard, S.: Assessment and improvement of the sea ice processing for dissolved inorganic carbon analysis, Limnol. Oceanogr. Methods, 16, 83–91, https://doi.org/10.1002/lom3.10229, 2018.

Huff, A. K. and Abbatt, J. P. D.: Kinetics and product yields in the heterogeneous reactions of HOBr with ice surfaces containing NaBr and NaCl, J. Phys. Chem. A, 106, 5279–5287, https://doi.org/10.1021/jp014296m, 2002.

Millero, F. J.: Chemical Oceanography, Fourth Edition, CRC Press, Boca Raton, 2013.

Moore, C. W., Obrist, D., Steffen, A., Staebler, R. M., Douglas, T. A., Richter, A. and Nghiem, S. V.: Convective forcing of mercury and ozone in the Arctic boundary layer induced by leads in sea ice, Nature, 506, 81–84, https://doi.org/10.1038/nature12924, 2014.

Oltmans, S. J. and Komhyr, W. D.: Surface ozone distributions and variations from 1973–1984: Measurements at the NOAA geophysical monitoring for climatic change baseline observatories, J. Geophys. Res., 91, 5229, https://doi.org/10.1029/jd091id04p05229, 1986.

Oltmans, S. J., Schnell, R. C., Sheridan, P. J., Peterson, R. E., Li, S. M., Winchester, J. W., Tans, P. P., Sturges, W. T., Kahl, J. D. and Barrie, L. A.: Seasonal surface ozone and filterable bromine relationship in the high Arctic, Atmos. Environ., 23, https://doi.org/10.1016/0004-6981(89)90254-0, 1989.

Platt, U. and Hausmann, M.: Spectroscopic measurement of the free radicals NO_3, BrO, IO, and OH in the troposphere, Res. Chem. Intermed., 20, https://doi.org/10.1163/156856794X00450, 1994.

Pratt, K. A., Custard, K. D., Shepson, P. B., Douglas, T. A., Pöhler, D., General, S., Zielcke, J., Simpson, W. R., Platt, U., Tanner, D. J., Gregory Huey, L., Carlsen, M. and Stirm, B. H.: Photochemical production of molecular bromine in Arctic surface snowpacks, Nat. Geosci., 6, 351–356, https://doi.org/10.1038/ngeo1779, 2013.

Raddatz, R. L. and Cummine, J. D.: Temporal surface ozone patterns in urban Manitoba, Canada, Boundary-Layer Meteorol., 99, 411–428, https://doi.org/10.1023/A:1018983012168, 2001.

Saiz-Lopez, A. and von Glasow, G.: Reactive halogen chemistry in the troposphere, Chem. Soc. Rev., 41, 6448–6472, https://doi.org/10.1039/c2cs35208g, 2012.

Schmidt, J. A., Jacob, D. J., Horowitz, H. M., Hu, L., Sherwen, T., Evans, M. J., Liang, Q., Suleiman, R. M., Oram, D. E., Le Breton, M., Percival, C. J., Wang, S., Dix, B. and Volkamer, R.: Modeling the observed tropospheric BrO background: Importance of multiphase chemistry and implications for ozone, OH, and mercury, J. Geophys. Res., 121, 11819–11835, https://doi.org/10.1002/2015JD024229, 2016.

Schroeder, W. H., Anlauf, K. G., Barrie, L. A., Lu, J. Y., Steffen, A., Schneeberger, D. R. and Berg, T.: Arctic springtime depletion of mercury, Nature, 394, 331–332, https://doi.org/10.1038/28530, 1998.

Simpson, W. R., von Glasow, R., Riedel, K., Anderson, P., Ariya, P., Bottenheim, J., Burrows, J., Carpenter, L. J., Frieß, U., Goodsite, M. E., Heard, D., Hutterli, M., Jacobi, H. W., Kaleschke, L., Neff, B., Plane, J., Platt, U., Richter, A., Roscoe,

https://doi.org/10.5194/acp-2021-157
Preprint. Discussion started: 22 March 2021


Atmospheric Chemistry and Physics Discussions

H., Sander, R., Shepson, P., Sodeau, J., Steffen, A., Wagner, T. and Wolff, E.: Halogens and their role in polar boundary-layer ozone depletion, Atmos. Chem. Phys., 7, 4375–4418, https://doi.org/10.5194/acp-7-4375-2007, 2007.

Simpson, W. R., Brown, S. S., Saiz-Lopez, A., Thornton, J. A. and von Glasow, R.: Tropospheric halogen chemistry: sources, cycling, and impacts, Chem. Rev., 115, 4035–4062, https://doi.org/10.1021/cr5006638, 2015.

Sjostedt, S. J. and Abbatt, J. P. D.: Release of gas-phase halogens from sodium halide substrates: Heterogeneous oxidation of frozen solutions and desiccated salts by hydroxyl radicals, Environ. Res. Lett., 3, https://doi.org/10.1088/1748-9326/3/4/045007, 2008.

Steffen, A., Schroeder, W., Macdonald, R., Poissant, L. and Konoplev, A.: Mercury in the Arctic atmosphere: An analysis of eight years of measurements of GEM at Alert (Canada) and a comparison with observations at Amderma (Russia) and Kuujjuarapik (Canada), Sci. Total Environ., 342, 185–198, https://doi.org/10.1016/j.scitotenv.2004.12.048, 2005.

Thomas, J. L., Stutz, J., Lefer, B., Huey, L. G., Toyota, K., Dibb, J. E. and von Glasow, R.: Modeling chemistry in and above snow at Summit, Greenland - Part 1: Model description and results, Atmos. Chem. Phys., 11, 4899–4914, https://doi.org/10.5194/acp-11-4899-2011, 2011.

Wang, F., Pućko, M. and Stern, G.: Transport and transformation of contaminants in sea ice, in Sea Ice: Third Edition, Edited by D.N. Thomas, John Wiley & Sons, pp. 472–491, https://doi.org/10.1002/9781118778371.ch19, 2017.

Wang, S., McNamara, S. M., Moore, C. W., Obrist, D., Steffen, A., Shepson, P. B., Staebler, R. M., Raso, A. R. W. and Pratt, K. A.: Direct detection of atmospheric atomic bromine leading to mercury and ozone depletion, Proc. Natl. Acad. Sci. U. S. A., 116, 14479–14484, https://doi.org/10.1073/pnas.1900613116, 2019.

Wu, S., Mickley, L. J., Jacob, D. J., Logan, J. A., Yantosca, R. M. and Rind, D.: Why are there large differences between models in global budgets of tropospheric ozone?, J. Geophys. Res. Atmos., 112, 1–18, https://doi.org/10.1029/2006JD007801, 2007.

Xu, W., Tenuta, M. and Wang, F.: Bromide and chloride distribution across the snow-sea ice-ocean interface: A comparative study between an Arctic coastal marine site and an experimental sea ice mesocosm, J. Geophys. Res. Ocean., 121, 5535–5548, https://doi.org/10.1002/2015JC011409, 2016.

Zhao, X., Strong, K., Adams, C., Schofield, R., Yang, X., Richter, A., Friess, U., Blechschmidt, A. M. and Koo, J. H.: A case study of a transported bromine explosion event in the Canadian high arctic, J. Geophys. Res., 121, 457–477, https://doi.org/10.1002/2015JD023711, 2016.